Available online at website: https://journal.bcrec.id/index.php/bcrec

Bulletin of Chemical Reaction Engineering & Catalysis, 21 (3) 2026, xxx-xxx

Original Research Article

Tailoring the Structural Evolution of Co-Supported Fibrous ZSM-5 via Hydrothermal Aging for Syngas Production in Ethanol Dry Reforming

Nor Shuhada Solehah Hanafi[1], Asmida Ideris[1], Aster Rahayu[2], Martomo Setyawan[2], Agus Aktawan[2], Herma Dina Setiabudi[1,3], Nurul Ainirazali[1,3*]

[1]Faculty of Chemical and Process Engineering Technology, Universiti Malaysia Pahang Al-Sultan Abdullah, 26300 Gambang, Pahang, Malaysia.
[2]Department of Chemical Engineering, Faculty of Industrial Technology, Universitas Ahmad Dahlan, Jl. Jend. Ahmad Yani, Banguntapan, Bantul, Yogyakarta, Indonesia 55166.
[3]Centre for Sustainable Fluid Energy Research (Fluid Energy), Universiti Malaysia Pahang Al-Sultan Abdullah, 26300 Gambang, Pahang, Malaysia.

Received: 14th March 2026; Revised: 28th April 2026; Accepted: 29th April 2026
Available online: 10th May 2026; Published regularly: October 2026

Abstract

The catalytic dry reforming of ethanol (EDR) offers a promising approach to reduce CO_2 emissions and support the less carbon-intensive processes. This study examined the effect of cobalt (Co) loading on fibrous ZSM-5 (FZSM-5), which was synthesized at hydrothermal aging times of 6, 8, and 10 h, for EDR. The catalytic evaluation was carried out at 650 °C, 1 bar, and 30,000 $mL.g^{-1}.h^{-1}$ for 8 h. The results showed that hydrothermal aging time influenced the catalyst properties and catalytic performance. The catalyst aged for 8 h developed a distinct dendritic structure, a surface area of 208.9 $m^2.g^{-1}$, and distributed hierarchical porosity. During EDR, the 8 h Co/FZSM-5 catalyst sustained stable ethanol conversion and produced a favorable H_2/CO ratio of 1.55. By contrast, the 6h catalyst showed low crystallinity, while the 10 h catalyst underwent extended crystal growth that limited mass transfer. TGA results further showed that the 8 h catalyst limited carbon deposition more effectively and exhibited less deactivation better than the other samples. These findings provide practical guidance for catalyst design and support the development of more resource-efficient reforming processes.

Keywords: Fibrous zeolite; Cobalt-based catalyst; Hydrothermal; H2/CO; Coke suppression; EDR; Dry reforming

How to Cite: Hanafi, N. S. S., Ideris, A., Rahayu, A., Setyawan, M., Aktawan, A., Setiabudi, H. D., Ainirazali, N. (2026). Tailoring the Structural Evolution of Co-Supported Fibrous ZSM-5 via Hydrothermal Aging for Syngas Production in Ethanol Dry Reforming. *Bulletin of Chemical Reaction Engineering & Catalysis*, 21 (3), xxx-xxx. (DOI: 10.9767/bcrec.20686)

Permalink/DOI: https://doi.org/10.9767/bcrec.20686

1. Introduction

Decarbonizing the chemical and fuel sectors hinges ona converting carbon dioxide (CO_2) from a liability into a feedstock. In 2024, energy-related CO_2 emissions edged up once again, reaching an estimated 37.8 Gt, an all-time high that underscores the scale of the challenge [1]. Yet that very carbon, once captured, can be rerouted through carbon-capture and utilisation (CCU) pathways to yield C1–C2 building blocks, fuels, and polymers. Central to almost every CCU value chain is synthesis gas (syngas), the adjustable mixture of H_2 and CO that underpins Fischer-Tropsch, methanol, ammonia, and oxo-alcohol platforms [2]. Currently, most industrial syngas is produced from coal gasification [3], steam reforming of natural gas [4], or partial oxidation of heavy hydrocarbons [5], and all three pathways linked to substantial carbon output and capital cost [6]. Consequently, advancing low-carbon

* Corresponding Authors.
Email: ainirazali@umpsa.edu.my (Ainirazali, N.)

syngas technologies is essential to achieve deep emissions reductions throughout downstream chemical value chains.

Dry reforming of ethanol, represented by the reaction, $C_2H_5OH + CO_2 \rightarrow 3CO + 3H_2$, presents a compelling route to low carbon syngas [7]. Compared with the traditional dry reforming of methane, ethanol dry reforming benefits from the higher hydrogen-to-carbon ratio of ethanol, which lowers the equilibrium temperature for syngas formation and greatly suppresses solid carbon deposition [8]. The process is strongly highly endothermic and genrally requires high operating temperature, typically 700 °C, to overcome kinetic constraints and reduce thermodynamic limitation [9]. However, highly active catalysts have been reported to deliver high H_2 yield at the lower temperature, such as 550 °C, by promoting reforming activity and suppressing competing side reaction [10]. Besides that, nickel (Ni)- and rhodium (Rh)-based catalyst systems can reach almost complete ethanol conversion with more than 90% hydrogen selectivity, yet they are constrained by noble-metal cost and limited hydrothermal durability [11]. Cobalt (Co) offers a plentiful, low-cost alternative with strong activity for carbon-carbon bond cleavage, but unmodified cobalt particles tend to sinter and promote filamentous carbon under dry reforming conditions [6,9,12].

ZSM-5 is widely utilized in catalysis and adsorption due to its distinctive channel system, form selectivity, hydrophobicity, strong acidity, and excellent thermal stability, making it a cost-effective material for diverse applications [13,14,15]. However, conventional compact zeolite crystals often face diffusion limitations, which can be mitigated by structural modifications such as forming fibrous zeolitic materials [16]. Fibrous ZSM-5 (FZSM-5) and Fibrous Faujasite Y (FY), for instance, exhibit an enhanced external surface area and better accessibility to active sites compared to their bulk counterparts, thereby improving mass transfer during reactions. FZSM-5 and FY were synthesized in this study via a hydrothermal-assisted microemulsion method followed by crystallization. Specifically, FZSM-5 was prepared by transferring the gel mixture into a Teflon-lined autoclave and treating it hydrothermally at 120 °C for 6 h [17], while FY was synthesized using a microemulsion system integrated with seed-assisted crystallization, followed by hydrothermal treatment at 120 °C for 6 h [18] and 12 h [19] to examine the effect of crystallization duration.

In hydrothermal synthesis, aging is an influential pre-crystallization step where the aluminosilicate gel is maintained at a regulated temperature, determining nucleation density, crystal growth, phase selectivity, and the formation of fibrous rather than compact morphologies. For ZSM-5, a silica-containing pentasil zeolite known for its fine-pore structure, large surface area, and distinct pore channel[16], increasing the aging time during hydrothermal treatment improved its crystallinity up to a maximum level [16]. Therefore, the aging and hydrothermal treatments play a pivotal role in controlling the formation and growth of ZSM-5 crystals, ultimately affecting structural properties and catalytic efficiency. Given this significance, further systematic study is warranted for structural modification and performance enhancement.

The use of cobalt was to maximize the catalytic efficiency while minimizing material usage [20,21]. Recently, it is proven that the noble metal including platinum, rhodium and ruthenium as well as non-noble metal as transition metal (Ni, Co and Fe), are employed a catalyst in EDR. Due to cheaper cost and equivalent catalytic efficiency, non-noble metal such as cobalt has been attracted in this research. Co-based catalyst, for instance, have notable soot oxidation capability, which can help improve resistance to carbon deposition by limiting coke formation during the reaction, However, cobalt catalyst is also highly susceptible to re-oxidation, which can lead to reduce catalytic performance [22]. Cobalt have been used in many application of industrial process, they are also active for dehydrogenation and oxidation reaction. Cobalt catalyst applied to partial oxidation of reaction 9 [23]. The addition of a non-noble metal is preferable. In this respect cobalt is of great interest [24]. Thus, this study focuses on systematically investigating the effect of hydrothermal aging time on the properties of fibrous ZSM-5 as support for Co loading, including the correlation between aging time, catalyst structure, and catalytic activity in the dry reforming of ethanol.

2. Materials and Method

2.1. Materials and Reagents

1-Butanol (≥ 98 %, Merck), toluene (≥ 98 %, Sigma-Aldrich), tetraethyl orthosilicate (TEOS, ≥ 99 %, Sigma-Aldrich), hexadecyltrimethyl-ammonium bromide (CTAB, ≥ 98 %, Sigma-Aldrich), urea (≥ 98 %, Merck), cobalt(II) nitrate hexahydrate $Co(NO_3)_2.6H_2O$ (≥ 98 %, Sigma-Aldrich) were used as received. Carbon dioxide, hydrogen, and nitrogen with a purity 99.99 % were supplied by Alpha Gas Solution Sdn. Bhd.

2.2. Synthesis of Fibrous ZSM-5 (F-ZSM-5) Support

A hydrothermal-assisted microemulsion route was used to prepare fibrous ZSM-5 (F-ZSM-5) [19]. First, 1-butanol and toluene were mixed at the desired weight ratio in a beaker. Then, pre-

formed ZSM-5 seeds were introduced, and the suspension was sonicated for one hour. Tetraethyl orthosilicate (TEOS) was added dropwise, and sonication continued for an additional hour to complete silica hydrolysis. A second solution containing water, CTAB, and urea was prepared separately under vigorous ultrasonic mixing until complete dissolution. The two solutions were combined, and the resulting mixture was sonicated at room temperature for four hours, followed by sonication in an 80 °C water bath for three hours. The slurry was transferred to a 250 mL Teflon-lined stainless-steel autoclave and heated at 120 °C for eight hours. After cooling, the solid product was recovered by centrifugation, washed with water to neutral pH, filtered, and dried overnight at 110 °C. Finally, the dried material was calcined in flowing air at 550 °C for 6 hours to remove organic templates and form the fibrous ZSM-5 support [18]. The hydrothermal aging time was varied from 6 to 10 hours, and the samples were designated as FZSM-5 XH, where X represents the time.

2.3. Preparation of Co/FZSM-5

The ultrasonic wet impregnation technique was employed to load transition metal cobalt (Co) active site onto fibrous zeolite (FZSM-5). A specific amount of cobalt nitrate hexahydrate ($Co(NO_3)_2.6H_2O$) was dissolved in deionized water and subsequently mixed with FZSM-5 [22]. The resulting mixture was heated in an ultrasonic water bath at 80 °C until most of the solvents evaporated. The obtained solid was then dried overnight at 110 °C and calcined at 550 °C for 6 hours. The resulting material was designed with a 3%Co/FZSM-5 XH.

2.4. Characterization Techniques

The textural properties, including specific surface area and pore characteristics, were determined via N_2 adsorption-desorption isotherms at 77 K using a Micromeritics ASAP-2010 analyzer, based on Brunauer-Emmett-Teller (BET) theory. The functional groups and metal-support interactions were assessed by Fourier-transform infrared (FTIR) spectroscopy, with spectra between 4000 and 400 cm^{-1} on finely ground powders pressed against the diamond crystal. Surface morphology was visualized by field-emission scanning electron microscopy (FESEM) (JEOL JSM-7800F). Carbon deposition and thermal stability were quantified by thermogravimetric analysis on a TGA analyzer in an air atmosphere containing 20% O_2 and 80% N_2, with the recording extending up to 750 °C .

2.5. Ethanol Dry Reforming (EDR)

Catalytic performance for Ethanol Dry Reforming (EDR) was evaluated in a stainless-steel fixed-bed reactor with an inner diameter of 11 mm and a total length of 417 mm, operated under ambient pressure. 0.1 g of catalyst, with a particle size range of 0.5-1.0 mm, was placed at the center of the reactor. Before the reaction, the catalyst was reduced in situ using a hydrogen flow of 50 mL/min at 700 °C for two hours[22]. Following the reduction step, a reactant gas mixture of ethanol and carbon dioxide (1:1 stoichiometric molar ratio) was introduced into the reactor at 650 °C [2], [9]. The reaction was conducted at a Gas Hourly Space Velocity (GHSV) of 30,000 mL g^{-1} h^{-1}, with a total of 8 hours of time-on-stream (TOS). Product gases at the reactor outlet were analyzed using Gas Chromatography with a Thermal Conductivity Detector (TCD) to determine conversion and product distribution. The ethanol conversion and product yield (H_2 and CO) were calculated based on the following equation: $C_2H_5OH + CO_2 \rightarrow 3CO + 3H_2$

Ethanol conversion:

$$x_{C2H6O}(\%) = \frac{(2 \times F_{H2}) + (4 \times F_{CH4})}{(6 \times F_{C2H5OH,in})} \times 100 \quad (1)$$

Product yield:

$$Y_{H_2}(\%) = \frac{(2 \times F_{H2})}{(6 \times F_{C2H5OH,in})} \times 100 \quad (2)$$

$$Y_{CO}(\%) = \frac{(F_{CO})}{\left(2 \times F_{C2H5OH,in}\right) + (F_{CO,in})} \times 100 \quad (3)$$

where, F represents the molar flow rate (mol/min).

3. Results and Discussion

3.1. Catalyst Characterization

3.1.1. N_2 adsorption-desorption analysis

The physical characteristics of 3%Co/FZSM-5 at various hydrothermal aging times were tabulated in Table 1. Among the catalysts, the 8 h hydrothermal treatment exhibits the highest BET surface area (208.91 m^2/g) with 0.1488 cm^3/g for pore volume, and 4.41 nm of pore diameter [18]. Meanwhile the 6 h sample exhibited a decline in BET area (≈15%) and pore volume (5.17%), but an increase in pore diameter (10.4%), yielding value of 177.86 m^2/g, 0.1411 cm^3/g, and 4.87nm, respectively. In contrast, extending the hydrothermal treatment for 10 h lead to in a 27.6% decrease in surface area relative to the 8h sample, despite a further increase in pore volume (16.8%), and pore diameter (51.5%) reaching 151.20 m^2/g, 0.1738 cm^3/g, and 6.68 nm, respectively. In a catalyst, a high surface area of the support materials provides a sufficient platform for uniform metal dispersion, effectively

preventing particle aggregation even at high metal loading [22]. Variations in textural properties across different hydrothermal durations show that the process alters the FZSM-5 structure. Research reports that aging time affects nucleation and crystallization rates, which in turn control crystal size and synthesis yield [25]. Consequently, the improvement in BET surface area and pore volume may result from a greater crystallinity within the catalyst. Meanwhile, prolonged hydrothermal aging time may initiate the dealumination of the FZSM-5 framework, resulting in localized framework collapse and a sharp reduction in both BET surface area and micropore volume [26]. While the total pore volume peaked at 10 h (0.1738 cm^3/g), increasing from 0.1411 cm^3/g for 6 h and 0.1488 cm^3/g for 8 h. This implies that while small micropore domains (which fell to 112.91 m^2/g at 10 h) collapsed or merged, the overall porosity continued to grow. Such textural modifications may influence EDR by altering cobalt dispersion, facilitating reactant diffusion, and enhancing active-site accessibility.

The N_2 adsorption/desorption isotherms and pore size distribution of FZSM-5 catalysts were plotted in Figure 1. This result reveals that the characteristics of the mesoporous FZSM-5, as evidence by the presence of hysteresis loop [27]. The capillary condensation of N_2 occurs over range of P/P= 0.4 and 0.9, demonstrating the existence of voids both inside and between the particles. This behavior confirms the occurrence of capillary condensation within the mesopores [28]. According to IUPAC categorization, the isotherm of all samples was classified as type IV multilayer adsorption at P/P_o= 0.4-0.8 between the mesopore range as isotherm plateaued. Type IV isotherm with a hysteresis loop, H3 represents the pore condensation and loop behavior between both adsorb-desorb branches, which usually reflects the features of mesoporous materials [29]. At low relative pressure (P/P_o <0.1), the initial uptake of N_2 in adsorption indicates the presence of microporosity an strong adsorbent-adsorbate interaction [27]. The fact that N_2 uptake occurs at low P/Po between 0.1 and 0.4 indicate that adsorption occurs on the surface of FZSM-5 catalyst, whereas at sharp increase uptake at P/Po between 0.8 and 1.0 is associated with capillary condensation in mesopores and interparticle voids of FZSM-5 [18].

Table 1. Physical attributes of 3%Co/FZSM-5 at different hydrothermal times.

Catalyst	BET Surface Area (m^2/g)	Pore Volume (cm^3/g)	Average Pore Diameter (nm)	Micropore Area (m^2/g)
3%Co/FZSM-5 6H	177.86	0.1411	4.87	124.07
3%Co/FZSM-5 8H	208.91	0.1488	4.41	129.49
3%Co/FZSM-5 10H	151.20	0.1738	6.68	112.91

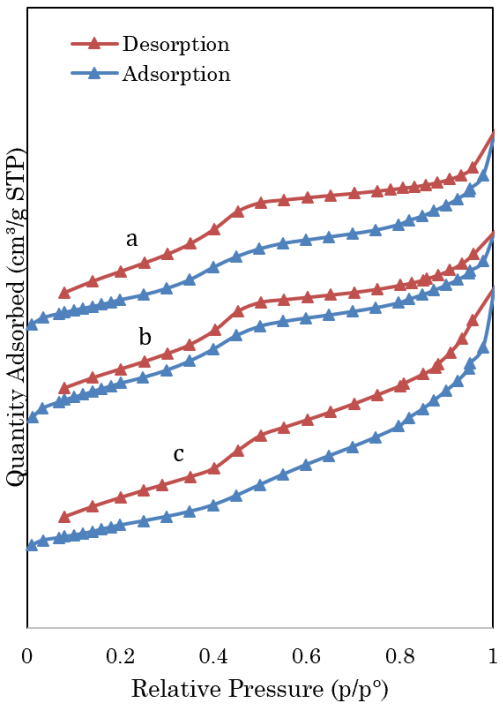

Figure 1. N_2 adsorption-desorption analysis for FZSM-5 (a) 6 h, (b) 8 h and (c) 10 h.

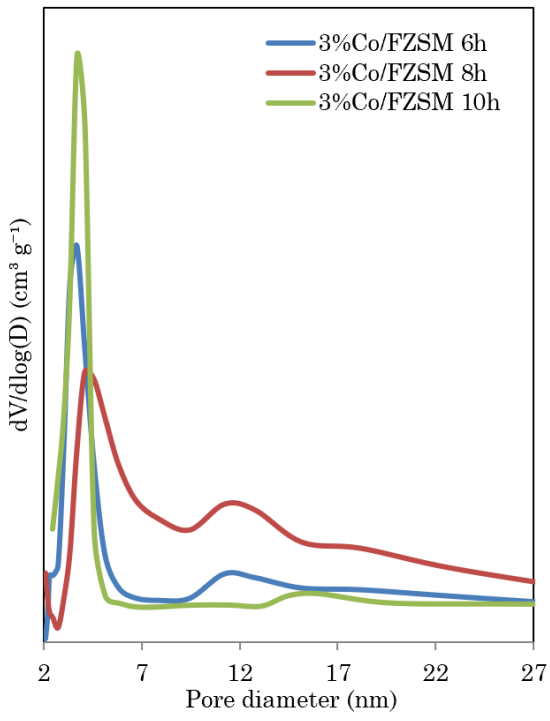

Figure 2. BJH desorption pore size distribution for 3%Co/FZSM-5.

The BJH pore size distribution was calculated from a branch of the nitrogen desorption isotherms. Figure 2 shows the BJH Desorption Pore Size Distribution of 3%Co/FZSM-5 catalyst. For 10 h, large peak was observed in the range of 2 nm to 5 nm, and the representative pore size was a maximum of around 4 nm. The presence of a distinct peak in this region indicates that mesopores contribute significantly to the pore structure of the catalyst [30]. The 10 h sample exhibits the sharpest and highest peak, indicating a more concentrated and uniform mesopore size distribution [18]. In contrast, the 8 h sample show a board distribution, suggesting a wider of mesopore size. Although 10 h has the most pronounced pore size distribution peak and the highest BHJ desorption pore volume, 8 h exhibits the highest BET surface area, indicating that pore size distribution and surface area do not necessarily vary in the same manner since large pore size can improve the mass transport and reduce coke accumulation in reaction part [18]. The influence of these textural properties on catalytic performance is discussed in details in reaction section.

3.1.2 Fourier-Transform Infrared Spectroscopy (FTIR) Analysis

The FTIR spectra of the 3%Co/FZSM-5 catalysts (400-4000 cm^{-1}) are shown in Figure 3. Within the framework vibration region (400-1300 cm^{-1}), the band at ≈540 cm^{-1}, common associated of the pentasil ring vibration, exhibits a gradual weakening with increasing hydrothermal duration. This attenuation suggests a partial loss of crystallinity and framework integrity, comparable to reports identifying such intensity reductions an indication of structural degradation and a loss-range order in aged ZSM-5 zeolites [25]. Furthermore, the modest shifts and intensity variations observed in the asymmetric Si-O-T stretching band (1050-1100 cm^{-1}) correspond to modifications in the Si/Al environment, in line with the occurrence of framework dealumination. In the hydroxyl stretching region (3000-3800 cm^{-1}), the band centered at ≈3610 cm^{-1}, assigned to the linking hydroxyl group (Si-OH-Al), shows progressive attenuation as aging duration increases. This trend points to a progressive loss of framework aluminum. In the content of the 3%Co/FZSM-5 catalysts, this decrease may also suggest an interaction between cobalt species and the acid sites. Such behavior is a hallmark of hydrothermal dealumination and is well-documented in studies concerning the steam-stabilization and degradation of zeolitic structures [18].

3.1.3 Field Emission Scanning Electron Microscopy (FESEM) Analysis

The morphological evaluation of the FZSM-5 samples with aging time is presented in Figure 4. All synthesized FZSM-5 samples exhibit a

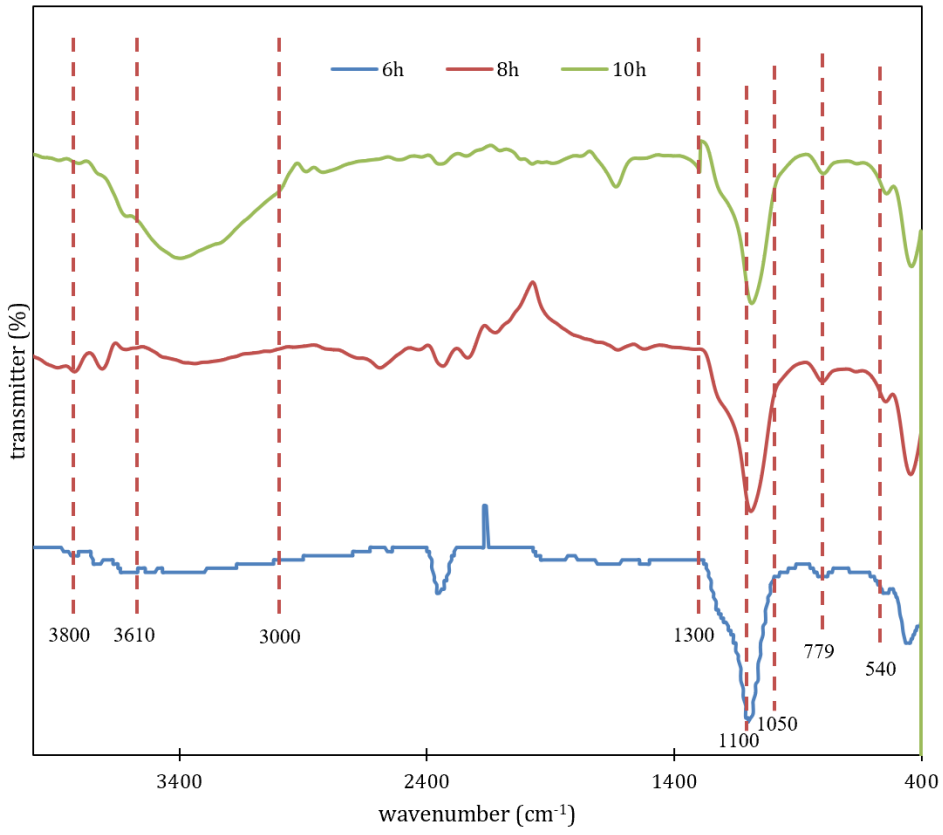

Figure 3. FTIR spectra for FZSM-5.

predominantly spherical "flower-like" distribution characterized by radical wrinkle morphologies. These particles closely resemble the dendritic fibrous nano-silica (KCC-1 type) structures reported in previous literature [31,32,33]. At the shortest aging time (6h), the particles exhibit predominantly irregular and poorly faceted morphologies. Spherical nuclei appear embedded within a dense, partially amorphous matrix. The absence of well-defined crystal edges and the presence of rounded, non-uniform particles indicate that FSMZ-5 crystallization is incomplete at this stage, where nucleation processes still dominate over crystal growth [17,34,35].

As the aging duration is prolonged to 8h, a uniform distribution of microspherical FZSM-5 aggregates was obtained. These aggregates are composed of clearly formed fibrous nanostructures, creating a hierarchical porosity with elevated crystallinity. The formation of this dendritic ZSM-5 was attributed to the interactive interaction among the urea surfactant, toluene, and the aqueous phase [36]. The absence of surface roughness produced to a homogeneous microporous framework [35]. The hierarchical structure combining micropores with notable wrinkles is associated with improved mass transport and promotes uniform cobalt dispersion. Furthermore, the increased surface area and available active sites allow greater interaction between reaction components [31] At extended hydrothermal aging times up to 10h, the crystallization appears complete, resulting in predominantly crystalline FZSM-5 crystals with no residual amorphous phase. However, the prolonged aging leads to a reduction in mesoporousity as the structure becomes gradually microporous and compact. The formerly defined fibrous features become less defined and extensively intergrown. This implies an overgrowth of the FZSM-5 crystals, leading to some loss of the hierarchical structure and a consolidated morphology [35]. This finding demonstrates that the morphology of FZSM-5 is closely related to the duration of the hydrothermal aging process, from a partially formed amorphous mixture at 6h, to a developed hierarchical dendritic structure at 8h, and finally to a highly intergrown crystal at extended aging times.

3.1.3 Thermogravimetric Analysis (TGA)

Figure 5 reveals the TG-DTG profiles with three distinct regimes of mass change for spent 3%Co/FZSM-5 catalysts aged at 6, 8, and 10 h. The baseline of fresh catalyst that provide the direct baseline for comparison, characteristic temperature range for moister removal and coke oxidation in ZSM-5 were refer from another journal. The TGA curves show two distinct stages of weight loss. The first stage (90 to 200 °C) is

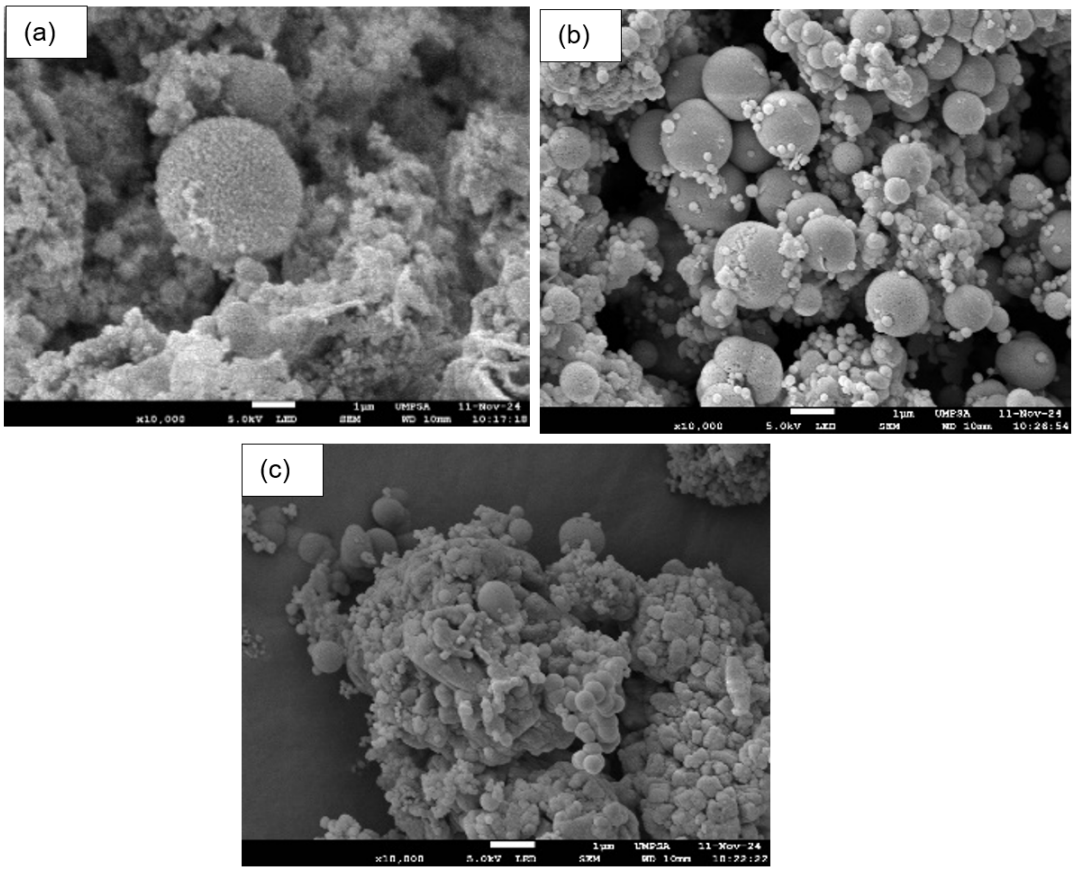

Figure 4. FESEM of FZSM-5 at different aging time (a) 6 h, (b) 8 h, (c) 10 h.

attributed to the removal of physically adsorbed water [37]. The second stage (550-800 °C) is more pronounced weight loss, corresponds to the combustion of coke deposited on catalyst during the cracking process [38]. There were All three samples lose a small amount of weight (<2 wt %) below 150 °C, attributable to the removal of physisorbed water and loosely bound volatiles. While a very gradual, nearly featureless decline in mass (<1 wt %) in the region 400 °C-625 °C was due to the oxidation of amorphous carbon species [18]. It was apparent that the weight loss at temperatures more than 625 °C is attributed to the combustion of thermally stable, graphitic coke [18]. Among the catalyst, the 8h hydrothermal aging time 3%Co/FZSM-5 exhibits the lowest weight loss, demonstrating superior coke resistance compared to the 6h and 10h sample due to its optimal fibrous structure and metal dispersion. The accumulated coke follows the order: 6 h (1.6 wt%) < 8 h (2.5 wt%)<10 h (4.2 wt%). The differences in coke formation were highly correlated with the Co/FZSM-5 catalysts' properties. Co/FZSM-5-6H catalyst has the highest BET surface area but relatively narrow pore size, which appears to restrict deep carbon growth, resulting in only a small fraction of coke remaining after the reaction. Meanwhile, for 8h aging catalyst, the structure with more open channels and hierarchical network intergrowth fibers allows deeper carbon penetration during the reaction, raising the coke formation to ~2.5 wt%. Prolonging aging to 10 h promotes coalescence of these spheres into denser cauliflower-like aggregates, which lowers BET surface area yet enlarges inter-particle channels seem to trap graphical fragments more effectively, culminating in the highest residual carbon. This result proven that an aging treatment time near 8 h offers an optimal compromise; sufficient surface area for activity, yet a morphology that restricts excessive coke deposition and facilitates its subsequent removal.

3.2. Catalytic Performance in Ethanol Dry Reforming (EDR)

The catalytic activity, stability, and product distribution of the 3%Co/FZSM-5 catalyst as a function of hydrothermal aging time are illustrated in Figure 6. The EDR was performed at 650 °C with a GHSV of 30,000 $mL.g^{-1}.h^{-1}$, and pressure atmosphere. Initial result indicates that the duration of hydrothermal aging during synthesis of FZSM-5 significantly impacts the structural properties of the catalyst, which in turn governs the catalytic activity of EDR. Initially, the catalyst hydrothermally aged for 10 hours exhibited a robust initial CO_2 conversion of approximately 80%. This elevated initial activity can be attributed to its expanded total pore volume (0.1738 cm^3/g), which facilitates the initial mass transfer and diffusion of CO_2 molecules to the active cobalt sites. However, the 10 h catalyst suffered from rapid deactivation, evidenced by a sharp decline in ethanol conversion to 55% within just 2 hours of time-on-stream (TOS). While the widened pores enhance initial reactant uptake, the concurrent reduction in microporosity (112.91 m^2/g) severely limits the catalyst's ability to

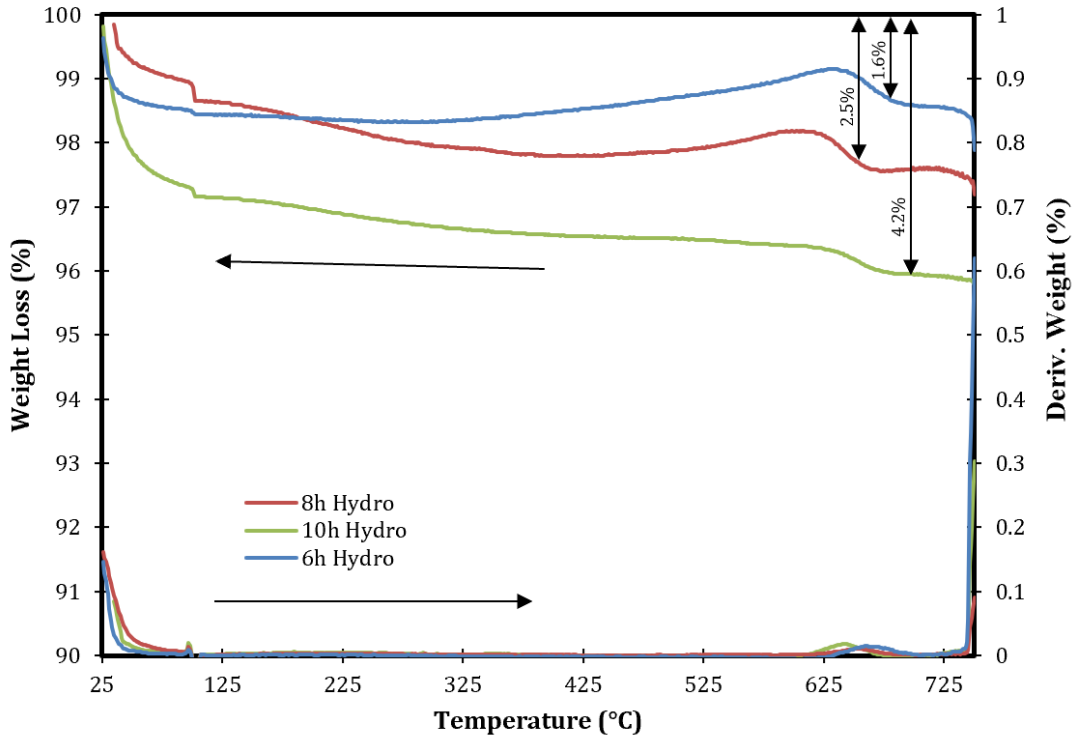

Figure 5. TG-DTG profiles of spent 3%CoFZSM-5 catalyst.

sustain reforming reactions, leading to rapid active site blocking. Ultimately, this loss of microporosity and pore widening lowers the overall density of active sites, thereby suppressing steady hydrogen production.

The 8 h catalyst showed the best long-term stability and overall reaction performance. Although its initial CO_2 conversion was marginally lower than that of the 10 h catalyst, it maintained the highest steady-state ethanol conversion (≈68%) and CO_2 conversion (≈60%) throughout the 8 h reaction. This stable performance is associated to its textural properties, particularly its higher BET specific surface area (208.91 m²/g) and larger measured microporosity (129.49 m²/g). These features improved cobalt dispersion and increase the number of accessible active sites. These also reduce deactivation by reducing coke formation and the poisoning effect of adsorbed water. It also notable that the catalyst properties influenced syngas distribution. The Co/FZSM-5 8 h catalyst showed the greatest steady-state hydrogen yield (≈55%), and the highest H_2/CO ratio (1.55), above those of the 6 h (0.9) and 10 h (1.3) catalysts. This result is related to the larger surface area and the specific radial wrinkle morphology of the FZSM-5 synthesized at 8 h, which promotes the formation of intermediate hydrocarbons and facilitates the formation of hydrogen molecules. Meanwhile, CO formation seems to be more favorable over the Co/FZSM-5 6H, due to its under-developed fibrous shell, which predominantly triggers ethanol dehydration pathways rather than the complete reforming reaction. With the Co/FZSM-5 10H, the reduction in microporosity and the widening of pores likely decrease the density of active sites, leading to inferior hydrogen production.

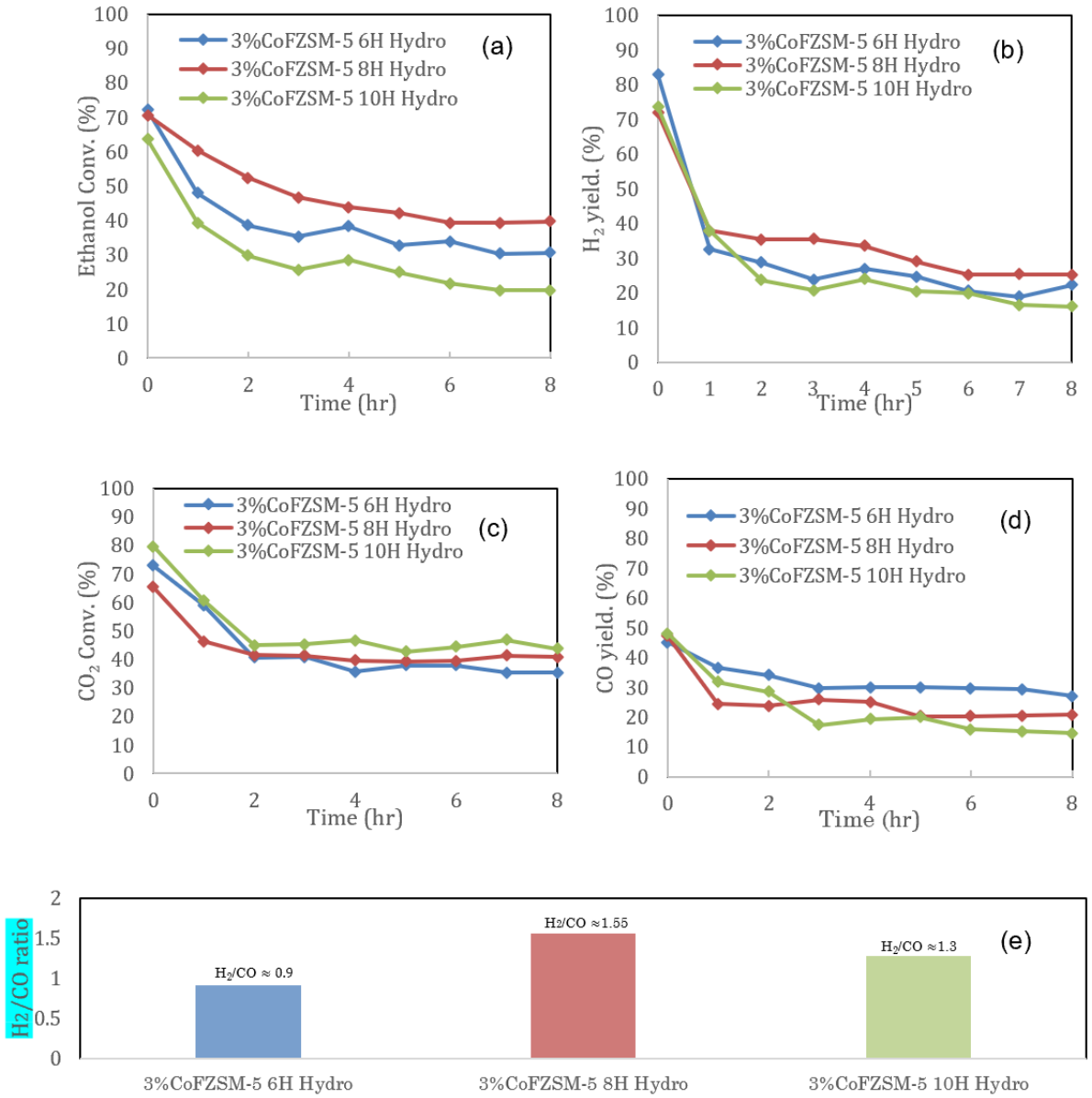

Figure 6. (a) Ethanol conversion, (b) H_2 yield, (c) CO_2 conversion, (d) CO yield and (e) H_2/CO ratio.

4. Conclusions

This study investigated the effect of ageing time on the morphology and catalytic properties of fibrous ZSM-5 (FZSM-5) supported cobalt catalyst for ethanol dry reforming (EDR). The 8h 3%Co/FZSM-5 produced the highest measured performance, achieving ethanol conversion of 68%, CO_2 conversion of 60%, and H_2 yield 55% with a syngas H_2/CO ratio of 1.55. Furthermore, the TGA analysis showed measurable coke accumulation, indicating that the sample with distinct dendritic morphology helps decrease deactivation by preventing pore-mouth plugging and stabilizing cobalt active sites against sintering. Conversely, the 10 h catalyst experienced increase deactivation rate due to its greater graphitic carbon deposition (4.2 wt%) and constrained microporosity. Thus, these findings suggest that hydrothermal aging is a controllable factor for modifying fibrous zeolites.

Acknowledgment

This work was funded by Universiti Malaysia Pahang Al-Sultan Abdullah under its Distinguished Research Grant (Project no. RDU 233011).

CRedit Author Statement

Author Contributions: Nor Shuhada Solehah Hanafi: Original draft, Methodology, Investigation, Formal Analysis, Data Curation, Nurul Ainirazali: Conceptualization, Validation, Supervision, Project Administration, Writing-review and editing, Asmida Ideris: Discussion, Writing-review and editing (Discussion development), Herma Dina Setiabudi: Discussion, Writing-review and editing (Discussion development) Aster Rahayu: Discussion, Discussion, Contributing Ideas, Martomo Setyawan: Funding Acquisition, Resources, Discussion, Contributing Ideas, Agus Aktawan: Funding Acquisition, Resources, Discussion, Contributing Ideas. All authors have read and agreed to the published version of the manuscript.

References

[1] Almulhim, A.I., Abubakar, I.R. (2026). The role of renewable energy in achieving the Sustainable Development Goals: A systematic review and conceptual framework. *Renewable and Sustainable Energy Reviews*, 230. DOI: 10.1016/j.rser.2025.116679.

[2] Li, T., Li, F., Nginyo, J., Cai, W., Yu, B. (2023). Syngas production through dry reforming of ethanol over Co@SiO_2 catalysts: Effect of SiO_2 shell thickness. *Molecular Catalysis*, 547(April) DOI: 10.1016/j.mcat.2023.113307.

[3] Dai, F., Zhang, S., Luo, Y., Wang, K., Liu, Y., Ji, X. (2023). Recent Progress on Hydrogen-Rich Syngas Production from Coal Gasification. *Processes*, 11. DOI: 10.3390/pr11061765.

[4] Alsudani, F.T., Saeed, A.N., Ali, N.S., Majdi, H.Sh., Salih, H.G., Albayati, T.M., Saady, N.M.C., Shakor, Z.M. (2023). Fisher–Tropsch Synthesis for Conversion of Methane into Liquid Hydrocarbons through Gas-to-Liquids (GTL) Process: A Review. *Methane*, 2(1), 24–43. DOI: 10.3390/methane2010002.

[5] Makaryan, I.A., Salgansky, E.A., Arutyunov, V.S., Sedov, I. V. (2023). Non-Catalytic Partial Oxidation of Hydrocarbon Gases to Syngas and Hydrogen: A Systematic Review. *Energies (Basel)*. 16. DOI: 10.3390/en16062916.

[6] Ay, H., Üner, D. (2015). Applied Catalysis B : Environmental Dry reforming of methane over CeO_2 supported Ni , Co and Ni – Co catalysts. *Applied Catalysis B, Environmental,*179, 128–138. DOI: 10.1016/j.apcatb.2015.05.013.

[7] Nguyen, A., Hoong, K., Senthil, P., Pham, T.T., Setiabudi, H.D., Yusuf, M., Kim, L., Pham, H., Thu, B.T., Abdul, A., Bin, M., Al-kahtany, K., Vo, D.N. (2024). Ceria-boosted Ni /Al_2O_3 catalysts for enhanced H_2 production via acetic acid dry reforming. *Journal of the Energy Institute*. 117(September), 1–12. DOI: 10.1016/j.joei.2024.101821

[8] Sub, B., Su, J., Sung, J., Choi, B., Jung, M., Kang, M. (2011). Hydrogen-rich gas production from ethanol steam reforming over Ni / Ga / Mg / Zeolite Y catalysts at mild temperature. *Applied Energy*, 88(12), 4366–4375. DOI: 10.1016/j.apenergy.2011.05.017.

[9] Nordin, M.I., Ideris, A., Azim Razat, M.S., Jamilatun, S., Pitoyo, J., Linarti, U., Ainirazali, N. (2026). Optimized Cobalt-Loaded Palm Oil Fuel Ash (Co/POFA) Catalyst for Syngas Production via Ethanol Dry Reforming. *Bulletin of Chemical Reaction Engineering & Catalysis*, 21(3), 507–515. DOI: 10.9767/bcrec.20662.

[10] Lang, L., Zhao, S., Yin, X., Yang, W. (2015). ScienceDirect Catalytic activities of K-modified zeolite ZSM-5 supported rhodium catalysts in low-temperature steam reforming of bioethanol. *International Journal of Hydrogen Energy*, 40(32), 9924–9934. DOI: 10.1016/j.ijhydene.2015.06.016.

[11] Mardwita, M., Yusmartini, E.S., Wisudawati, N. (2020). Effects of cobalt and chromium loadings to the catalytic activities of supported metal catalysts in methane oxidation. *Bulletin of Chemical Reaction Engineering & Catalysis*, 15(1), 213–220. DOI: 10.9767/bcrec.15.1.6320.213-220.

[12] Grzybek, G., Greluk, M., Patulski, P., Stelmachowski, P., Tarach, K., Słowik, G., Rotko, M., Valencia, S., Rey, F., Góra-Marek, K. (2023). Adjustment of the ZSM-5 zeolite support towards the efficient hydrogen production by ethanol steam reforming on cobalt catalysts. *Chemical Engineering Journal*, 467 DOI: 10.1016/j.cej.2023.143239.

[13] Jouini, H., de Marcos-Galán, A., Mejri, I., Bensouilah, R., Mhamdi, M., Blasco, T., Delahay, G. (2022). Understanding the Catalytic Deactivation upon Hydrothermal Aging at 850 °C of WO_3/Fe-Cu-ZSM-5 Catalyst for Selective Catalytic Reduction of NO by NH3. *Inorganics*, 10(11) DOI: 10.3390/inorganics10110180.

[14] Liu, Y., Bolshakov, A., Ćoza, M., Drozhzhin, V., Hensen, E.J.M., Kosinov, N. (2023). Isomorphously Substituted [Fe,Al]ZSM-5 Catalysts for Methane Dehydroaromatization. *ACS Catalysis*, 13(12), 8128–8138. DOI: 10.1021/acscatal.3c00854.

[15] Wang, C., Aztiria, T., Rzepka, P., Verel, R., Xu, J., Deng, F., van Bokhoven, J.A., Paunović, V. (2024). Structural Changes of ZSM-5 Catalysts during Methanol-to-Hydrocarbons Conversion Processes. *ACS Catalysis*, 14(16), 12410–12424. DOI: 10.1021/acscatal.4c02625.

[16] Chen, Y., Cong, S., Wang, Q., Han, H., Lu, J., Kang, Y., Kang, W., Wang, H., Han, S., Song, H., Zhang, J. (2018). Optimization of crystal growth of sub-micron ZSM-5 zeolite prepared by using $Al(OH)_3$ extracted from fly ash as an aluminum source. *Journal of Hazardous Materials*, 349, 18–26. DOI: 10.1016/j.jhazmat.2018.01.004.

[17] Abdullah, N., Ainirazali, N., Hanafi, N.S.S., Setiabudi, H.D., Chin, S.Y., Mohamed, A.R., Jalil, A.A. (2024). Glycerol dry reforming over Ni supported on fibrous ZSM5 and ZY: Correlation of structural properties on H_2 production. *Chemical Engineering Research and Design*, 209, 358–366. DOI: 10.1016/j.cherd.2024.08.012.

[18] Bahari, M.B., Jalil, A.A., Mamat, C.R., Arifin, M.A., Hassan, N.S., Alhassan, M., Sawal, M.H., Izzudin, N.M., Hatta, A.H., Aziz, M.A., Prasetyoko, D., Rajendran, S. (2024). Optimizing hydrogen-driven n-pentane isomerization over Pt-doped fibrous ZSM-5. *Molecular Catalysis*, 557(February), 113951. DOI: 10.1016/j.mcat.2024.113951.

[19] Lin, X., Qu, W., Wang, Z., Liu, J., Qian, C., Tian, L., Wang, L., Zhang, Y., Zhou, H., Zhao, Y., Wu, Y. (2025). Decoding heterogeneous electrocatalysts for acidic oxygen evolution: mechanisms, rational design and AI acceleration. *Natl. Sci. Rev.* 12. DOI: 10.1093/nsr/nwaf474.

[20] Cai, Q., Meng, Y., Wu, C., Qu, W., Wang, Q., Li, T., Liu, C., Chen, J., Lin, H., He, Q., Zhao, Y., Xi, S., Lu, J. (2025). De-Saturation of Single-Atom Copper Catalysts for Accelerating Propargylic Substitution Reactions. *Advanced Materials*, 37(50), DOI: 10.1002/adma.202509221.

[21] Owgi, A.H.K., Jalil, A.A., Aziz, M.A.A., Nabgan, W., Alhassan, M., Sofi, M.H.M., Hassan, N.S., Saravanan, R., Bahari, M.B. (2024). Methane dry reforming on fibrous silica-alumina employing nanocrystals of nickel and cobalt to recognize the most efficient metal. *International Journal of Hydrogen Energy*, 52, 567–579. DOI: 10.1016/j.ijhydene.2023.05.004.

[22] Mardwita, M., Yusmartini, E.S., Wisudawati, N. (2020). Effects of cobalt and chromium loadings to the catalytic activities of supported metal catalysts in methane oxidation. *Bulletin of Chemical Reaction Engineering & Catalysis*, 15(1), 213–220. DOI: 10.9767/bcrec.15.1.6320.213-220.

[23] Ay, H., Üner, D. (2015). Dry reforming of methane over CeO_2 supported Ni, Co and Ni-Co catalysts. *Applied Catalysis B: Environmental*, 179, 128–138. DOI: 10.1016/j.apcatb.2015.05.013.

[24] Nguyen, D.K., Dinh, V.P., Dang, N.T., Khan, D.T., Hung, N.T., Thi Tran, N.H. (2023). Effects of aging and hydrothermal treatment on the crystallization of ZSM-5 zeolite synthesis from bentonite. *RSC Advances*, 13(30), 20565–20574. DOI: 10.1039/d3ra02552g.

[25] Wang, A., Lindgren, K., Di, M., Bernin, D., Carlsson, P.A., Thuvander, M., Olsson, L. (2020). Insight into hydrothermal aging effect on Pd sites over Pd/LTA and Pd/SSZ-13 as PNA and CO oxidation monolith catalysts. *Applied Catalysis B: Environmental*, 278, DOI: 10.1016/j.apcatb.2020.119315.

[26] Chong, C.C., Abdullah, N., Bukhari, S.N., Ainirazali, N., Teh, L.P., Setiabudi, H.D. (2019). Hydrogen production via CO_2 reforming of CH_4 over low-cost Ni/SBA-15 from silica-rich palm oil fuel ash (POFA) waste. *International Journal of Hydrogen Energy*, 20815–20825. DOI: 10.1016/j.ijhydene.2018.06.169.

[27] Jesudoss, S.K., Vijaya, J.J., Kaviyarasu, K., Kennedy, L.J., Jothi Ramalingam, R., Al-Lohedan, H.A. (2018). Anti-cancer activity of hierarchical ZSM-5 zeolites synthesized from rice-based waste materials. *RSC Advances*, 8(1), 481–490. DOI: 10.1039/c7ra11763a.

[28] Lang, L., Zhao, S., Yin, X., Yang, W., Wu, C. (2015). Catalytic activities of K-modified zeolite ZSM-5 supported rhodium catalysts in low-temperature steam reforming of bioethanol. *International Journal of Hydrogen Energy*, 40(32), 9924–9934. DOI: 10.1016/j.ijhydene.2015.06.016.

[29] Izzudin, N.M., Jalil, A.A., Ali, M.W., Aziz, F.F.A., Azami, M.S., Hassan, N.S., Fauzi, A.A., Ibrahim, N., Saravanan, R., Hassim, M.H. (2022). Promoting a well-dispersion of MoO_3 nanoparticles on fibrous silica catalyst via one-pot synthesis for enhanced photoredox environmental pollutants efficiency. *Chemosphere*, 308 DOI: 10.1016/j.chemosphere.2022.136456.

[30] Ghani, N.N.M., Jalil, A.A., Triwahyono, S., Aziz, M.A.A., Rahman, A.F.A., Hamid, M.Y.S., Izan, S.M., Nawawi, M.G.M. (2019). Tailored mesoporosity and acidity of shape-selective fibrous silica beta zeolite for enhanced toluene co-reaction with methanol. *Chemical Engineering Science*, 193, 217–229. DOI: 10.1016/j.ces.2018.09.009.

[31] Li, S., Jiang, X., Sun, H., He, S., Zhang, L., Shao, L. (2019). Mesoporous dendritic fibrous nanosilica (DFNS) stimulating mix matrix membranes towards superior CO_2 capture. *Journal of Membrane Science*, 586, 185–191. DOI: 10.1016/j.memsci.2019.05.069.

[32] Dos Santos, M.B., Vianna, K.C., Pastore, H.O., Andrade, H.M.C., Mascarenhas, A.J.S. (2020). Studies on the synthesis of ZSM-5 by interzeolite transformation from zeolite Y without using organic structure directing agents. *Microporous and Mesoporous Materials*, 306 DOI: 10.1016/j.micromeso.2020.110413.

[33] Karim, T.M., Toyoda, H., Sawada, M., Zhao, L., Wang, Y., Xiao, P., Wang, L., Huang, J., Yokoi, T. (2024). Aluminum Distribution on the Microporous and Hierarchical ZSM-5 Intracrystalline and Its Impact on the Catalytic Performance. *Chem and Bio Engineering*, 1(9), 805–816. DOI: 10.1021/cbe.4c00117.

[34] Hambali, H.U., Jalil, A.A., Triwahyono, S., Jamian, S.F., Fatah, N.A.A., Abdulrasheed, A.A., Siang, T.J. (2021). Unique structure of fibrous ZSM-5 catalyst expedited prolonged hydrogen atom restoration for selective production of propylene from methanol. *International Journal of Hydrogen Energy*, 46(48), 24652–24665. DOI: 10.1016/j.ijhydene.2019.11.236.

[35] Izhab, I., Amin, N.A.S., Asmadi, M. (2017). Dry reforming of methane over oil palm shell activated carbon and ZSM-5 supported cobalt catalysts. *International Journal of Green Energy*, 14(10), 831–838. DOI: 10.1080/15435075.2017.1334659.

[36] Ravandi, R., Khoshbin, R., Karimzadeh, R. (2018). Synthesis of free template ZSM-5 catalyst from rice husk ash and co-modified with lanthanum and phosphorous for catalytic cracking of naphtha. *Journal of Porous Materials*, 25(2), 451–461. DOI: 10.1007/s10934-017-0457-3.